nanomaterials

MDPI

Article

Modeling and Characterization of Stress Relaxation Behavior of EVA–CNT Nanocomposites Under Uniaxial Loading

Felicia Stan [1,*], Stefanut Ciochina [2,*], Ionut-Laurentiu Sandu [1] and Catalin Fetecau [1]

[1] Center of Excellence Polymer Processing, Dunarea de Jos University of Galati, 47 Domneasca, 800008 Galati, Romania; laurentiu.sandu@ugal.ro (I.-L.S.); catalin.fetecau@ugal.ro (C.F.)
[2] Faculty of Sciences and Environment, Dunarea de Jos University of Galati, 47 Domneasca, 800008 Galati, Romania
* Correspondence: felicia.stan@ugal.ro (F.S.); stefanut.ciochina@ugal.ro (S.C.)

Abstract

Understanding the time-dependent viscoelastic behavior of polymer carbon nanotube (CNT) nanocomposites is crucial for predicting their performance, particularly in load-bearing applications where the nanocomposites can be exposed to either short- or long-time loadings. In this study, the stress relaxation behavior of ethylene-vinyl acetate (EVA)–CNT nanocomposites containing 1, 3, and 5 wt% CNTs was experimentally investigated under load- and strain-controlled uniaxial relaxation conditions and modeled using the generalized Maxwell linear viscoelastic model. The results indicate that in the linear viscoelastic domain, the EVA–CNT nanocomposites retain at least 70–80% of their instantaneous modulus, and the equilibrium modulus almost doubled with increasing nanotube content from 1 to 5 wt%, yielding a 1.70- to 1.85-fold increase depending on the initial strain and relaxation period. When the strains exceed the viscoelastic limit (10–25%), all nanocomposites relaxed to about 65–70% of the initial stress. The generalized Maxwell model accurately captured the relaxation behavior of EVA–CNT nanocomposites within the linear viscoelastic domain, providing a robust fit for experimental relaxation data with relative errors not exceeding 5%. This study expands the potential application of EVA–CNT nanocomposites in engineering by providing insights into their stress relaxation behavior under both small and large deformations while highlighting areas for future improvement.

Keywords: stress relaxation; Maxwell model; Prony parameters; polymer nanocomposites; carbon nanotubes; EVA

Check for updates

Academic Editor: Teresa Cuberes

Received: 11 September 2026
Revised: 27 October 2026
Accepted: 1 November 2026
Published: 4 November 2026

Copyright: © 2026 by the authors. Licensee MDPI, Basel, Switzerland. This article is an open access article distributed under the terms and conditions of the Creative Commons Attribution (CC BY) license.

1. Introduction

Polymer carbon nanotube (CNT) nanocomposites are advanced materials obtained by dispersing CNTs into a polymer matrix. The unique structural, electrical, and mechanical properties of CNTs make polymer CNT nanocomposites a promising candidate for a broad range of applications [1–8]. When CNTs are added to a polymer, depending on the selection of the polymer matrix and CNT content, in addition to the enhanced mechanical performance [2,4,5,8], the resulting nanocomposites can also gain electrical conductivity [4,8,9], better thermal stability [4,6,9], and electromagnetic shielding capability [1,10]. Therefore, research and development efforts are being made to engineer polymer CNT nanocomposites with properties that meet the specific demands of specific applications, such as aerospace (lightweight, lighting-strike resistance) [4,7,8], automotive (high-strength, weight-reduction) [4,8], electronics (flexibility, piezo-resistivity, electromagnetic interface

shielding) [1,10], and biomedical areas (large surface area, functionalization, flexibility and durability, conductivity) [3,5,7].

In the case of structural nanocomposite parts used in engineering applications, the main goal is the improvement of mechanical performance while preserving the processability of the polymer matrix [4,8]. However, most studies dealing with the mechanical behavior of polymer CNT nanocomposites are limited to time-independent behavior, although, in practice, polymer CNT nanocomposite components may exhibit time-dependent (viscoelastic) deformations such as stress relaxation [11–22] and creep [11,23–26].

In polymer-based composites, the time-dependent viscoelastic behavior is affected not only by the polymer matrix but also by filler content, filler dispersion, and agglomeration, with the addition of fillers generally slowing down the relaxation process [13,14,19,27,28]. Depending on the nature of the polymer matrix and filler content, several mechanisms can occur during the stress relaxation process, such as the breakage or disruption of the filler–filler and filler–polymer networks, the disentanglement of polymer-polymer networks, or the pullout of fillers from the polymer matrix [5,13,14,26,28,29].

In general, during the short-term relaxation of polymer CNT nanocomposites, the dominant mechanism is polymer segmentation motion, while the medium-term relaxation process is governed by interfacial relaxation. The polymer chains that are absorbed directly onto the CNT surfaces (bound layers) have restricted mobility, dictating the energy dissipation and viscoelastic transitions at intermediate time scales [24,29]. However, the long-term relaxation process is based on the rearrangement of the CNT network [16,26].

At small CNT content (well below the percolation threshold), CNTs act as physical obstacles, and the polymer chain motion becomes partially restricted; therefore, the relaxation rate decreases. When CNT content approaches the network threshold, the stress transfer efficiency increases since the nanotubes form interconnected structures that act as restricting sites; therefore, CNT–polymer interfacial interactions and chain slippage become more difficult. At higher CNT loadings, the relaxation process becomes much slower, and the nanocomposite behaves more like a solid (long-term residual stress increases) [13,16].

One promising application of polymer CNT nanocomposites is in electronics. In recent years, significant progress has been achieved in the development of polymer CNT nanocomposites with enhanced sensing properties, making them suitable to be used in monitoring devices for a wide range of applications, particularly for flexible strain sensors [14,30–35]. The strain sensing capacity of polymer CNT nanocomposites is governed by the change in electrical resistance relative to the applied strain [14,30–35]. Therefore, during strain sensing, the polymer CNT nanocomposites are subjected to external stimuli (small and large deformations), which create the potential for stress relaxation [14,15,19,30–35].

Ethylene-vinyl acetate (EVA) and CNTs are generally combined to create flexible, lightweight nanocomposites with improved properties [36–49], which are used in engineering applications such as flexible electronics, strain sensors, smart textiles, and soft robotics [37,40–47]. For these applications, in addition to sensitivity, which is a prerequisite, understanding stress relaxation behavior under different loading conditions is essential to avoid failures during service. However, most studies on EVA–CNT nanocomposites focus on the mechanical properties under quasi-static [36,38,39,42,49] or piezoresistive loading conditions [36–47], while the research on the time-dependent viscoelastic behavior is still insufficient. Therefore, this study investigates the stress relaxation behavior of EVA–CNT nanocomposites with 1, 3, and 5 wt% CNTs. To assess and establish the difference between the three formulations, uniaxial tensile stress relaxation tests were conducted in a wide range of applied loads and strains. The mechanisms involved in the relaxation process were analyzed using the generalized Maxwell linear viscoelastic model.

2. Experimental

2.1. Material and Sample Preparation

The nanocomposites considered in this study consist of the ethylene-vinyl acetate (EVA) copolymer (Alcudia PA-420, Repsol [50]) with 20% vinyl acetate, reinforced with 1, 3, and 5 wt% thin-multi walled carbon nanotubes (CNT, NC7000™, Nanocyl S.A., Sambreville, Belgium) [51]. These CNT concentrations were selected to ensure good processability while preserving the mechanical properties of EVA matrix, particularly the ductility. The EVA–CNT nanocomposites, supplied by Nanocyl S.A. (Belgium), were prepared by melt mixing. According to the manufacturer, the nanotubes were directly incorporated into the molten polymer (140 °C) via a side feeder. The test specimens (Type I according to ISO-527 [38,52]) were manufactured by injection molding using an Arburg injection molding machine (Allrounder 320, Arburg, Lossburg, Germany). The injection molding parameters were set as follows: 140 °C melt temperature, 30 °C mold temperature, 70 MPa injection pressure, 15 cm^3/s injection speed, 10 s holding time, and 20 s cooling time.

2.2. Stress Relaxation Tests

For the current study, to investigate the time-dependent relaxation behavior of the EVA–CNT nanocomposites, load- and strain-controlled uniaxial relaxation tests were performed on a universal testing machine (M350-AT, Testometric Co. Ltd., Rochdale, UK) with a displacement reading resolution of 0.001 mm with 0.025 N accuracy. The stress relaxation tests were performed at room temperature with a crosshead speed of 50 mm/min, and three fresh specimens were used for each relaxation test. Before stress relaxation testing, uniaxial tensile tests were conducted at a crosshead speed of 50 mm/min to evaluate the mechanical properties (e.g., elastic modulus and yield point) and estimate the upper limit of the linear viscoelastic region (LVR). The stress–strain curves were determined directly from the load-crosshead displacement curves.

In the load-controlled relaxation tests, the specimens were stretched to the same initial load level (50 and 100 N, respectively, to ensure that the stress measurements remain within the elastic zone or near the yield point). After reaching the predefined load, the crosshead was held constant at the corresponding strain level, and the force was monitored for a time span of 12 h.

In the strain-controlled relaxation tests, i.e., a linear ramp to a prescribed strain, the specimens were stretched to a predefined strain (1, 10, and 25%) with the same crosshead displacement of 50 mm/min. Following the ramp loading to the defined strain level, the crosshead was stopped, and the specimen was held over a time span of 1 h while the force was monitored. It should be noted that the initial strains of 10% and 25% were selected to investigate the stress relaxation behavior under large strains since—in many engineering applications—the relaxation response may occur outside the LVR.

3. Modeling of Stress Relaxation Behavior

3.1. Generalized Maxwell Model

The constitutive model used to describe the viscoelastic behavior of EVA–CNT nanocomposites is based on the generalized Maxwell model that consists of a spring of elastic modulus E_∞ in parallel with Maxwell elements [18,53–55], as shown in Figure 1.

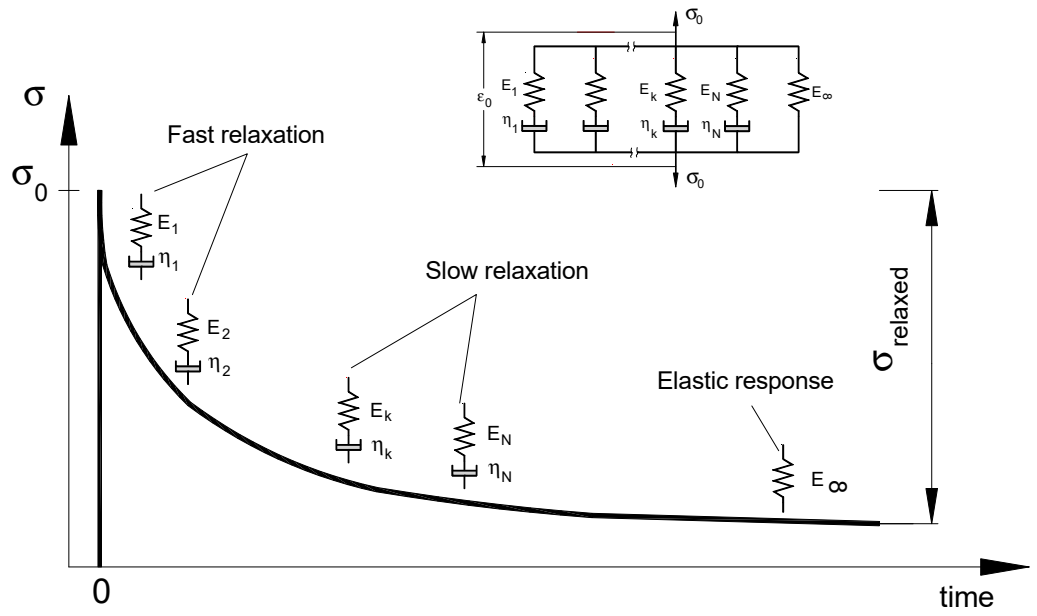


Figure 1. Stress relaxation curve and the generalized Maxwell model with relaxation elements connected in parallel.

Since the elements of the generalize Maxwell model are connected in parallel, the strain $\varepsilon(t)$ is identical across all elements (branches), while the total stress $\sigma(t)$ splits among them. Thus, the total relaxation stress can be expressed as follows [53,54]:

$$\sigma(t) = \sigma_\infty + \sum_{k=1}^{N} \sigma_k \exp\left(-\frac{t}{\tau_k}\right) \tag{1}$$

where σ_∞ is the long-term equilibrium stress, σ_k is the stress contribution of the k-th Maxwell element, and N is the number of Maxwell elements.

In linear viscoelasticity, for uniaxial stress relaxation under applied constant strain, the time-dependent behavior can be described by the relaxation modulus given by the following equation [53,54]:

$$E(t) = \frac{\sigma(t)}{\varepsilon_0} \tag{2}$$

where ε_0 is the initial constant strain (step strain).

The relaxation modulus is generally given in the form of Prony series [53,56,57].

$$E(t) = E_\infty + \sum_{k=1}^{N} E_k \exp\left(-\frac{t}{\tau_k}\right) \tag{3}$$

where E_∞ is the-long term equilibrium relaxation modulus (as $t \to \infty$), $\tau_k = \eta_k / E_k$ is the k-th relaxation time (relaxation time spectrum), and E_k is the k-th Prony coefficient (relaxation modulus, spring/stiffness constants of the k-th Maxwell element). The values τ_k and E_k form a discrete relaxation spectrum.

The instantaneous modulus, or the glassy modulus (as $t = 0$), is given by the following equation [54]:

$$E_0 = E_\infty + \sum_{k=1}^{N} E_k \tag{4}$$

In the case of polymer CNT nanocomposites, each term in the Prony series represents a mechanism occurring at a specific time scale, such as chain (segmental) motion, polymer chain disentanglement, CNT network rearrangement including CNT–CNT and polymer–CNT breakage, or interfacial slippage and debonding [11,13,16,23]. Segmental motion and

chain disentanglement are two mechanisms specific to the polymer matrix. Since CNTs introduce a large interfacial area where polymer chains are constrained [24,29], polymer chains near the CNT surface have restricted mobility, i.e., the CNT network creates delayed relaxation behavior. On the other hand, the load is transferred from the polymer matrix to CNTs and back to the polymer; thus, interfacial slipping or debonding can occur over time [16,23].

Small τ values (e.g., fast relaxation process, short-term relaxation) describe the segmental motion of polymer chains; while the response of the polymer matrix dominates the relaxation behavior, the CNTs have a minimal contribution. Medium τ values (e.g., intermediate-term relaxation) describe interfacial effects or disentanglement. In this case, the contribution of the CNTs to the relaxation process increases. An interphase zone forms around the nanotubes where polymer chains are tightly adsorbed or pinned to the CNT walls [24,29]. This chain immobilization delays the relaxation process, causing the nanocomposite to hold onto stress longer than the neat polymer. Long-term relaxation (larger τ values) is generally characterized by two mechanisms: interfacial slipping and CNT network rearrangement. In this case, the effect of CNTs is dominant. Under continuous uniaxial tension, the polymer matrix relaxes intensively, transferring the load to the CNT network. If the strain is high enough, interfacial sliding occurs at the polymer–CNT interface due to weak van der Waals forces. Simultaneously, the percolated CNT network undergoes structural rearrangement, slowly breaking and reforming contact points to release energy [11,13,16].

The values of τ_k and E_k can be estimated by minimizing the least-squares error to fit a set of experimental data with Equation (3) for $2N$ unknown parameters.

The initial guess for the relaxation times τ_k in Equation (3) can be estimated using the approach proposed by Ref. [58]:

$$\tau_k = \tau_1 \cdot 10^{(k-1)\cdot\Delta} \tag{5}$$

where

$$\Delta = \log\left(\frac{\tau_{\max}}{\tau_{\min}}\right) \cdot \frac{1}{N-1} \tag{6}$$

in which $\tau_{\min}$ and $\tau_{\max}$ are the first and last available data durations of the relaxation experiment.

As the number of the Maxwell elements increases, approaching infinity ($N \to \infty$), the relaxation function (3) can be expressed in integral form [56,59]:

$$E(t) = E_\infty + (E_0 - E_\infty) \cdot \int_0^\infty h(\tau) \cdot \exp\left(-\frac{t}{\tau}\right) d\tau \tag{7}$$

where $h(\tau)$ represents the continuous relaxation time spectrum.

For convenience in the computation, the relaxation function (7) can be normalized by the difference $E_0 - E_\infty$, leading to [56,59]:

$$R(t) = \frac{E(t) - E_\infty}{E_0 - E_\infty} = \int_0^\infty h(\tau) \cdot \exp\left(-\frac{t}{\tau}\right) d\tau \tag{8}$$

The integral (8) can be solved by utilizing an inverse Laplace transform.

The long-term relaxation ratio is defined as:

$$R_\infty = \frac{\sigma_0 - \sigma_\infty}{\sigma_0} \cdot 100\% \tag{9}$$

It can be computed to describe the experimental relaxation behavior at time $t = \infty$.

3.2. Prony Parameter Fitting

The parameters of the generalized Maxwell model, used to study the viscoelastic behavior, are calculated in MATLAB (R2025a) using the nonlinear least-squares method [60]. The mathematical algorithm consists of minimizing the sum of squares of the residuals between the experimental data and those obtained by the developed model [54,60]

$$C = \frac{\sum_{i=1}^{M}\left(E_i^{\exp} - E_i^{fit}\right)^2}{\sum_{i=1}^{M}\left(E_i^{\exp}\right)^2} \quad (10)$$

where $E_i^{\exp}$ and E_i^{fit} denote the experimental and predicted modulus, and M is the number of time points.

The residuals were calculated in logarithmic space, providing a more balanced weighting across the time domain. Additionally, a series of constraints were imposed on the model optimization. The first condition refers to the positivity of the equilibrium modulus and the elastic moduli, and the second restriction is given by the fact that the relaxation times must be within the time interval used in the experimental part. The objective function minimization uses the Trust Region Reflective algorithm [60], in accordance with the restrictions imposed.

The reliability and accuracy of the model were evaluated by calculating the coefficient of determination (R^2) and the sum of squares (SSq) of the relative error. The SSq was used as an overall measure of the error of the predicted model.

The range of relaxation times for the fitting process should be the same as the range of measured data, or about a decade or two larger than the complete range of experimental data, as shown by Ref. [61]. To model the viscoelastic behavior with Prony series, at least one relaxation time per decade—equally spaced along the logarithmic time axis—should be taken. Moreover, it was shown that two relaxation times per decade yield some improvement, while considering more than two relaxation times per decade will not bring any substantial improvement into the quality of fitting [59,61,62].

4. Results and Discussion

4.1. Morphology of EVA–CNT Nanocomposites

Figure 2 displays the SEM images of the cryo-fractured samples of EVA nanocomposites with 1, 3, and 5 wt% CNTs. Depending on the CNT content, an analysis of SEM images highlights three main characteristics in the EVA–CNT nanocomposite morphology: isolated CNTs, CNT bundles, and CNT agglomerates.

At the lower content (1 wt%), CNTs (bright spots) are dispersed randomly in the form of isolated (single) nanotubes and small bundles (Figure 2a). Also, it is observed that CNTs are wrapped by a large amount of the EVA matrix and primarily oriented along the flow direction (perpendicular to the cross-section). At 3 wt%, in addition to isolated CNTs and CNT bundles, small CNT agglomerates are visible (Figure 2b). At 5 wt%, the number of CNT agglomerates increased, and between these agglomerates, loosely connected CNTs and even isolated CNTs are observed (Figure 2c).

Comparing the SEM images of nanocomposite samples with different CNT contents, no major differences in the size of CNT agglomerates were observed, which are roughly 1–3 μm in diameter; this could be attributed to high shear forces developed during the injection molding process [38,39], which break down the bigger CNT agglomerates that may exist in pellets and could not be dispersed during the melt mixing process. These results are similar with other results reported in the literature [14,23,26,36,63].

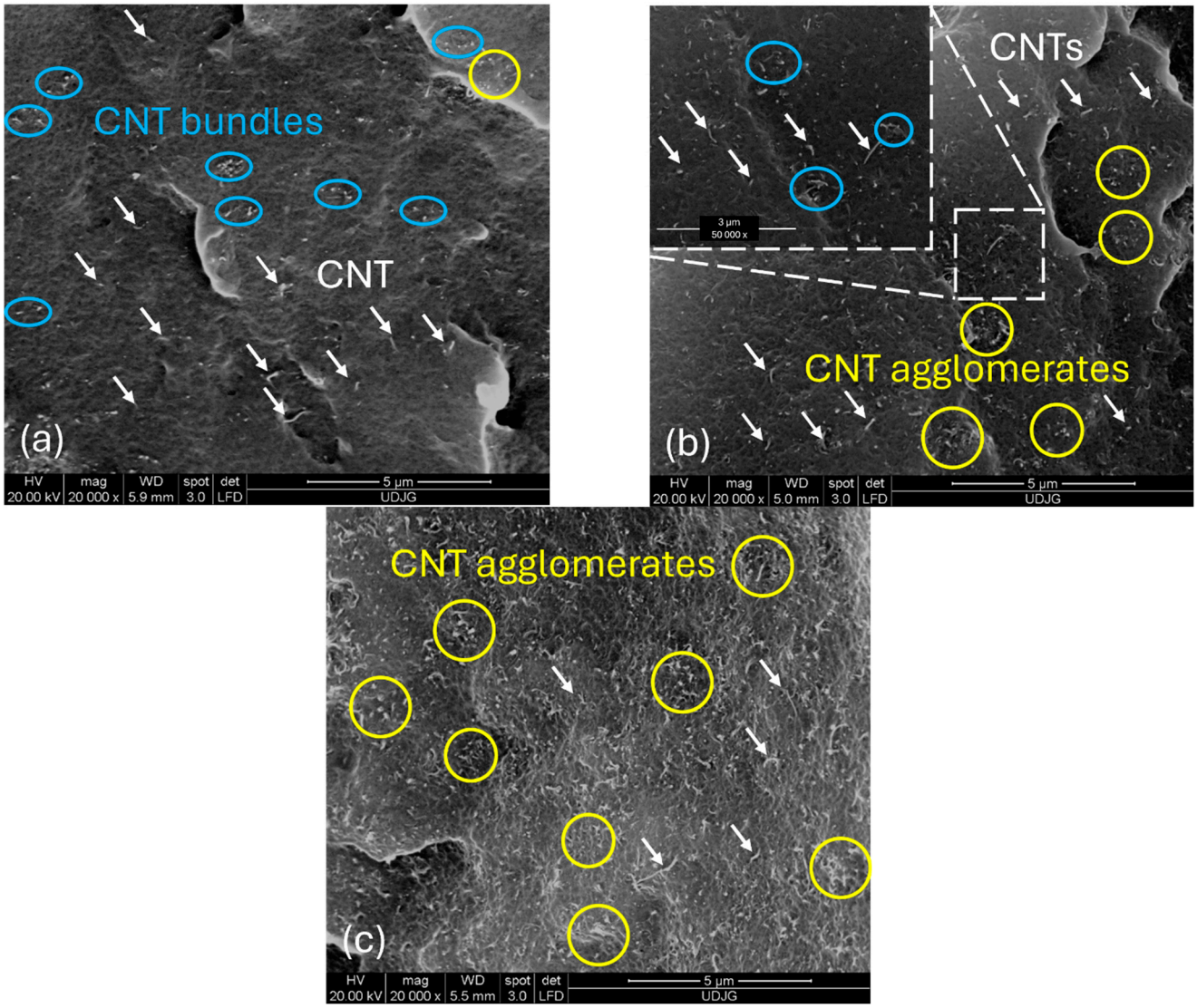


Figure 2. SEM image of EVA–CNT nanocomposite with (**a**) 1 wt%, (**b**) 3 wt%, and (**c**) 5 wt% CNTs.

4.2. Relaxation Behavior of EVA–CNT Nanocomposites

4.2.1. Classification of Relaxation Behavior

Figure 3 shows representative nominal stress–strain curves for the EVA–CNT nanocomposite as a function of the CNT content. All nanocomposites exhibit a bi-linear stress–strain relationship without a pronounced yield point. The overall load-bearing capacity increases with increasing CNT content, accompanied by an increase in linear elastic zone (i.e., proportional limit) and elastic limit (i.e., the point where material begins to experience nonlinear deformation), as well as a decrease in yielding (i.e., 2% offset deformation) and ductility (i.e., strain at break). An evaluation of the elastic moulus, i.e., the slope of the stress–strain curve in the elastic region, yielded values of 54, 72, and 92 MPa for 1, 3 and 5 wt% CNT, respectively.

Based on the experimental data in Figure 3, two relaxation regions were identified depending on whether the nanocomposite response is (i) in the linear viscoelastic region (LVR, below the yield point) or (ii) in the non-linear viscoelastic region (non-LVR, above the yield point).

Since the EVA–CNT nanocomposites do not present a sharp, distinct yield point, the upper limit of the LVR was defined as the 2% offset yield strain, which reached 9.8, 8.2,

and 6.9% for 1, 3, and 5 wt% CNTs, respectively. Hence, for the load-controlled tests, the response is linear viscoelastic (corresponding to initial strains up to 6%), whereas, for the strain-controlled tests, the response is linear viscoelastic at 1% strain and becomes nonlinear viscoelastic at 10% and 25% strain.

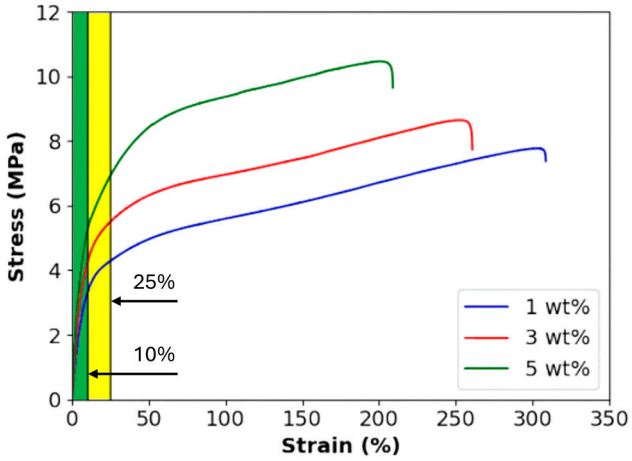


Figure 3. Stress–strain curves for EVA–CNT nanocomposites.

4.2.2. Load-Controlled Stress Relaxation Behavior of EVA–CNT Nanocomposites

Figure 4 shows the typical stress relaxation curves for the EVA–CNT nanocomposite as a function of CNT content for the two initial loads of 50 N and 100 N. Zero time was taken as the time when the crosshead was stopped—the maximum prescribed load was reached. The relaxation stress was calculated under the assumption that no changes in the cross-section area occur during the relaxation test. The parameters related to the relaxation of EVA–CNT nanocomposites (e.g., the initial stress, σ_0, initial strain, ε_0, equilibrium stress, σ_∞, and relaxation ratio, R_∞) are presented in Table 1.

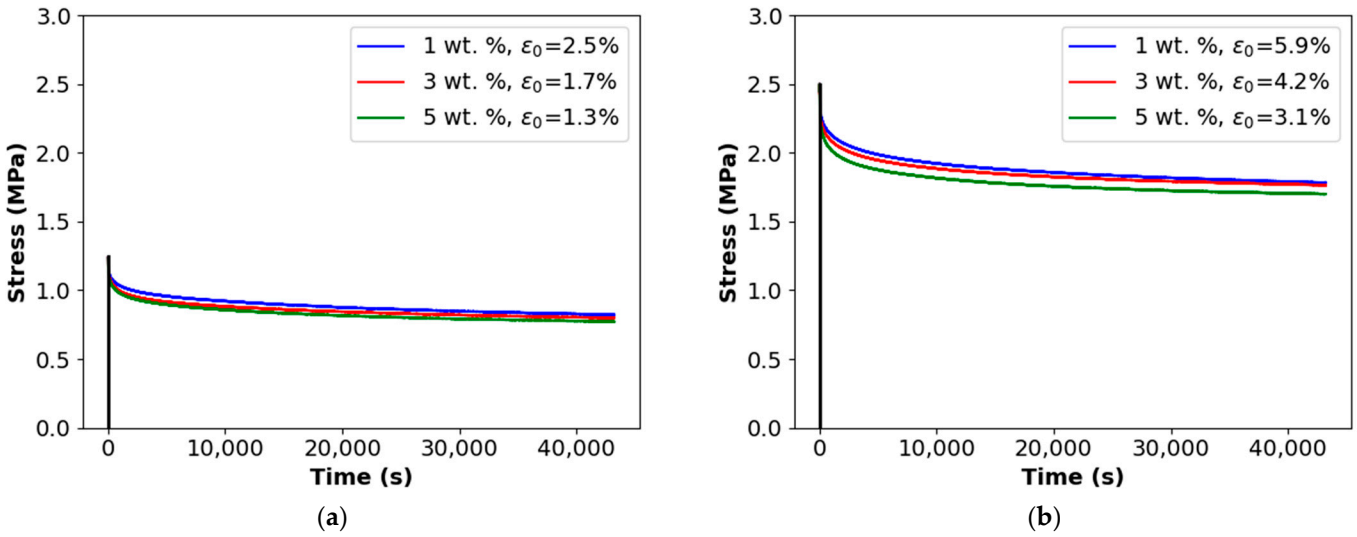


Figure 4. Stress relaxation response of EVA–CNT nanocomposites after stretching to an initial load of (**a**) 50 N and (**b**) 100 N.

As illustrated in Figure 4, the relaxation of EVA–CNT nanocomposites occurs gradually, reaching a steady state after about 1 h of relaxation and decreased by only 15% and 10% for initial loads of 50 N and 100 N, respectively, after being held for 12 h. Moreover, the EVA–CNT nanocomposites relaxed to different stress levels depending on the initial loading (initial strain), and none of them relaxed completely. It is also observed that the initial

relaxation strain decreases with increasing CNT content as the material becomes more rigid (Table 1).

Table 1. Summary of stress relaxation data for EVA–CNT nanocomposites—load-controlled test.

Initial Load (N)	σ_0 (MPa)	ε_0 (%)	CNTs (wt%)	σ_∞ (MPa)	R_∞ (%)
50	1.25	2.5 ± 0.05	1	0.82 ± 0.0007	34.4
		1.7 ± 0.08	3	0.80 ± 0.0004	36.0
		1.3 ± 0.07	5	0.77 ± 0.0004	38.4
100	2.5	5.9 ± 0.04	1	1.78 ± 0.002	28.8
		4.2 ± 0.11	3	1.76 ± 0.001	29.6
		3.1 ± 0.05	5	1.70 ± 0.001	32.0

To further analyze the effect of CNTs on stress relaxation, the normalized stress obtained for the first 100 s was plotted in Figure 5. Stress relaxation is likely governed by fast, local segmental motion of the polymer chains and CNTs do not locally influence the short-range relaxation. Consequently, the normalized stress curves overlap. As the relaxation time increases, the polymer chains interact with CNTs, and the curves start to separate.

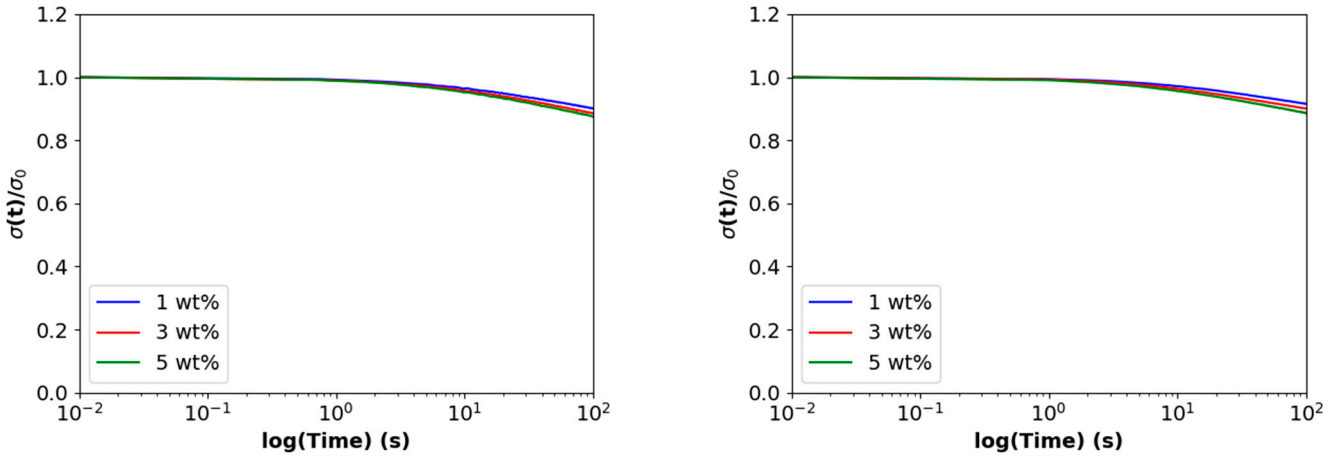


Figure 5. Normalized stress relaxation response of EVA–CNT nanocomposites after stretching 100 s to an initial load of (**a**) 50 N and (**b**) 100 N.

As can be seen in Table 1, the nanocomposite with 1 and 3 wt% CNTs retains a slightly higher percentage of its initial stress as compared with 5 wt% CNTs. On the other hand, increasing CNT content from 1 to 5 wt% increases the relaxation ratio after 12 h, indicating that the nanocomposite with 5 wt% relaxes faster than the nanocomposite with 1 and 3 wt% CNTs, meaning that the material dissipates more internal stress over time when held at a constant strain.

The stress relaxation behavior is hypothesized to be governed by several competing mechanisms that, generally, are activated depending on the applied load/strain and CNT content. At low CNT content (e.g., 1 wt%), the polymer matrix dominates the relaxation process as CNTs are likely isolated or form weak, sparse pathways (Figure 2a). As the content increases to 3 wt%, CNTs form a percolation network, while higher CNT content (e.g., 5 wt%) creates a denser, percolating network (Figure 2c). Under constant strain during a 12 h relaxation period, this dense network may potentially undergo physical structural rearrangement—such as inter-tube or polymer–CNT interfacial sliding, CNT–CNT junction breakage, or network reorganization, as documented in the literature [11–13,23,26,64,65].

This provides an additional pathway for stress dissipation that does not exist at lower CNT contents, leading to lower equilibrium stress (higher relaxation at equilibrium, Table 1). On the other hand, due to the high aspect ratio, at higher CNT content (5 wt%), the total surface area of the nanotubes interacting with the polymer matrix increases; when the nanocomposite is held at constant strain, the polymer chain segments experience localized shear forces against the CNT surfaces. The energy is dissipated through interfacial friction and micro-slippage between the polymer matrix and nanotubes, increasing the relaxation ratio [11,13,24,29]. Moreover, higher filler contents may increase the mobility of the amorphous phase due to CNT acting as restricted sites [65], or it may introduce microscopic defects and void [25,66,67], allowing the polymer matrix surrounding the nanotubes to relax more rapidly.

When the load doubles from 50 to 100 N (e.g., the initial stress doubles from 1.25 to 2.5 MPa), the nanocomposites show better long-term performance as they retain a higher percent of the initial stress and relax slower after 12 h (e.g., the relaxation ratio decreases, Table 1), but the tendency with CNTs remains the same. Doubling the initial load causes a sharp increase in the initial elastic stress response, while the viscous component of the material has a physical limit of how fast it can dissipate that energy. On the other hand, when the initial load is doubled, the polymer chains are stretched out. The localized stress concentrations lock the neighboring polymer chains tightly against the rigid CNT walls [24,29]. Under continuous loading, these trapped polymer segments are immobilized, preventing rearrangement or sliding, which restricts viscoelastic relaxation [21,24,29].

Statistical analysis indicates a highly significant effect of the initial relaxation load on the long-term relaxation stress (p-value = 0.0001), whereas the influence of CNT content is marginal (p-value = 0.06) at the 5% significance level.

To obtain the relaxation parameters that can be used for further predictions, the experimental relaxation data in Figure 4 were modeled using the generalized Maxwell model, as shown in Equation (3), by minimizing the least-squares coefficient (Equation (10)). Although the ramp loading is not an ideal ramp, the experimental ramp time was about 15 s, the effect of ramp history was neglected [57,61,68,69]. According to Ref. [68], the ramp data can be ignored if the experimental relaxation time is more than 100 times larger than the ramp time. In this case, the relaxation modulus, obtained from the relaxation response after the ramp, is a good approximation of the true relaxation modulus.

The experimental data cover about 4.5 decades; thus, in this analysis, it was determined that five Prony terms give a good fitting to the stress relaxation data. During the fitting procedure, the values of the relaxation times were fixed at equal intervals along the logarithmic time scale, and only the associated coefficients were determined by minimizing Equation (10). It should be noted that the initial guesses for τ_k were estimated based on Equations (5) and (6), and then refined to 1 s, 10 s, 10^2 s, 10^3 s, and 10^4 s.

The Prony parameters obtained through curve fitting (Equation (10)) for the ideal step loading—i.e., neglecting the ramp loading part—are given in Tables 2 and 3. It should be noted that the instantaneous modulus E_0 was computed with Equation (4). The experimental relaxation modulus and the numerical predictions using the Maxwell model with five elements are illustrated in Figure 6. The predicted relaxation modulus has been separated by one decade for clarity. The Maxwell model captures very well the relaxation in EVA nanocomposites ($R^2 \approx 0.98$ to 0.997). The maximum relative error between the experimental and predicted values falls to under 5%.

Table 2. Maxwell parameters of EVA–CNT nanocomposites—the ideal step with 50 N initial loading.

k	τ_k (s)	E_k (MPa)		
		1 wt%	**3 wt%**	**5 wt%**
1	1	1.15	1.75	2.44
2	10	0.36	1.09	2.04
3	10^2	5.33	8.39	11.79
4	10^3	1.90	4.61	6.35
5	10^4	7.72	9.99	14.54
E_∞ (MPa)		33.47	47.55	61.87
E_0 (MPa)		49.94	73.37	99.03
R^2		0.982	0.9872	0.991
SSq		1.978	1.305	0.225

Table 3. Maxwell parameters of EVA–CNT nanocomposites—the ideal step with 100 N initial loading.

k	τ_k (s)	E_k (MPa)		
		1 wt%	**3 wt%**	**5 wt%**
1	1	8.89×10^{-2}	1.5×10^{-2}	0.76
2	10	1.27	2.77	3.30
3	10^2	3.02	4.13	7.32
4	10^3	2.14	3.48	5.50
5	10^4	5.29	6.66	9.03
E_∞ (MPa)		30.48	41.98	56.07
E_0 (MPa)		42.29	59.04	81.98
R^2		0.994	0.996	0.997
SSq		0.639	0.338	0.306

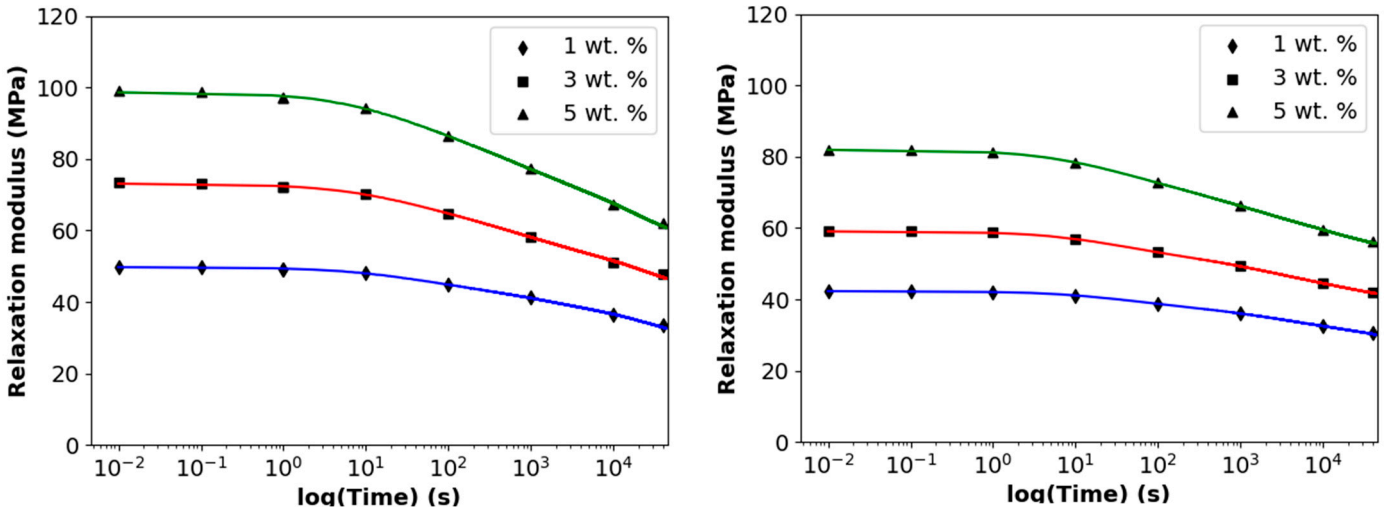


Figure 6. Predicted (symbols) and experimental (solid lines) relaxation modulus of EVA–CNT nanocomposites: (**a**) 50 N and (**b**) 100 N initial loading.

Under both loading conditions, both the instantaneous modulus E_0 and equilibrium modulus E_∞ of the EVA nanocomposite increase substantially as the CNT content increases from 1 to 5 wt%. In fact, these values almost doubled (Tables 2 and 3), showing clear mechanical reinforcement. The increase in both the instantaneous modulus and long-term

equilibrium modulus may indicate that CNTs formed a percolated network that restricts the free movement of flexible EVA chain segments [38,39].

The absolute drop in modulus during the relaxation process ($\Delta E = E_0 - E_\infty$) is more than double, indicating that introducing more CNTs increases the total amount of stress energy that the nanocomposite can dissipate over time. Moreover, the relative relaxed modulus ($\Delta E/E_0$) increases steadily with increasing CNT content. For example, at 50 N, the $\Delta E/E_0$ increased from about 33 to 38% as the CNT content increased from 1 to 5 wt%. On the other hand, the $\Delta E/E_0$ decreases when the EVA nanocomposites are subjected to higher loads; for instance, at 5 wt% CNTs, it drops from about 38% at 50 N to 32% at 100 N. At 100 N, the EVA nanocomposite is stretched towards the upper limit of the elastic zone, activating more CNTs to sustain the load. The large deformation of the matrix may induce higher interfacial shear stress across the polymer–CNT interface [13,24,65], slightly restricting molecular slippage over 12 h. Additionally, under long-term high deformations, CNTs can potentially slip, and the CNT network is prone to breaking, which reduces their reinforcing efficiency [13,24,65].

4.2.3. Strain-Controlled Relaxation Behavior of EVA–CNT Nanocomposites

The representative stress relaxation curves for the EVA–CNT nanocomposites stretched to different initial tensile strains (1, 10, and 25%) are presented in Figure 7. Zero time was taken at the time when the prescribed strain value was reached, and the crosshead was stopped. Table 4 presents the corresponding stress relaxation parameters.

Table 4. Summary of stress relaxation data for EVA–CNT nanocomposites—strain-controlled test.

ε_0 (%)	CNTs (wt%)	σ_0 (MPa)	σ_∞ (MPa)	R_∞ (%)
1	1	0.63 ± 0.003	0.51 ± 0.018	19.05
	3	0.87 ± 0.009	0.69 ± 0.007	20.69
	5	1.04 ± 0.071	0.88 ± 0.010	15.38
10	1	3.45 ± 0.04	2.56 ± 0.039	25.80
	3	4.23 ± 0.030	2.91 ± 0.081	31.21
	5	5.15 ± 0.044	3.55 ± 0.088	31.07
25	1	4.24 ± 0.034	2.86 ± 0.050	32.55
	3	5.53 ± 0.276	3.61 ± 0.196	34.72
	5	6.71 ± 0.124	4.48 ± 0.003	33.23

The initial relaxation stress σ_0 and the long-term equilibrium stress σ_∞ increased with increasing initial strain and nanotube wt%, as can be seen in Table 4. At each initial strain level, the σ_0 value increased due to the reinforcing effect of CNTs; the higher the nanotube wt% is, the higher the initial stress. This indicates that the external loads are efficiently transferred to the nanotubes in terms of shear stress through the CNT–EVA interface. Furthermore, at each initial strain level, the nanocomposite containing 5 wt% CNTs retained a greater σ_∞ value after 1 h compared to those with 1 and 3 wt% CNTs.

When the first 100 s of the experimental relaxation data were analyzed (Figure 8a), it was observed that at 1% initial strain, the normalized stress curves overlap regardless of the nanotube content. This behavior is likely due to the fact that the EVA matrix relaxes at its intrinsic rate. As the relaxation time increased, the polymer chain slipping interacts with CNTs and the curves start to separate. At higher initial strains (10% and 25%), the overlapping zone reduced substantially, indicating that the polymer matrix is stressed out and CNTs start to contribute to the relaxation process event at very short relaxation times (Figure 8b,c).

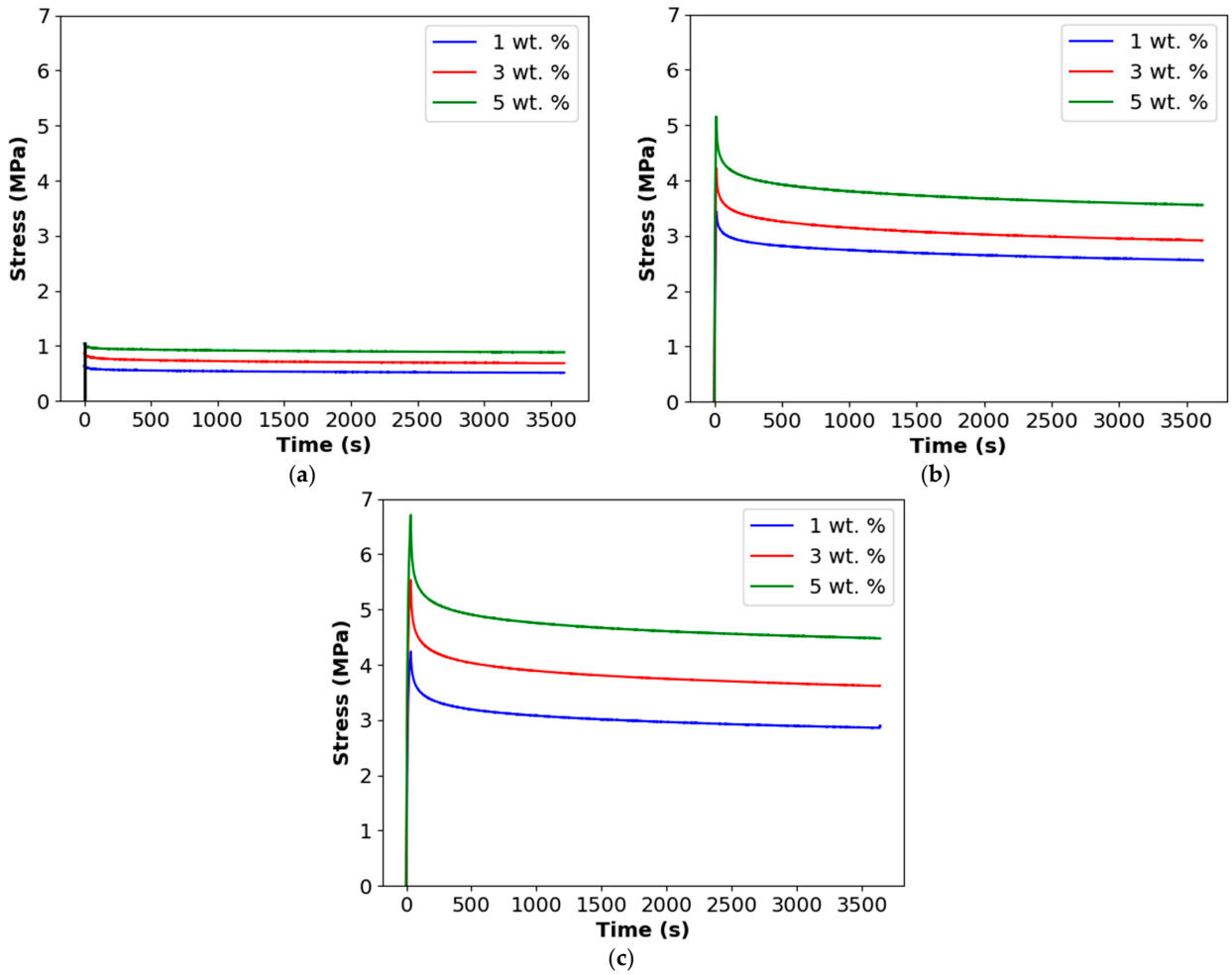


Figure 7. Stress relaxation response of EVA–CNT nanocomposites after stretching to (**a**) 1%, (**b**) 10%, and (**c**) 25% initial strain.

Table 4 indicates that the relaxation ratio increases with increasing initial strain, suggesting that the nanocomposites relax faster at higher initial strains. At 1% initial strain, although a higher CNT content provides superior reinforcement, the nanocomposites with 1 and 3 wt% exhibit faster relaxation compared to the 5 wt%.

At 25% initial strain, the nanocomposite with 5 wt% CNTs exhibited higher initial and equilibrium stresses after 1 h. However, the differences in the stress relaxation ratios among the three CNT contents were negligible, with all nanocomposites relaxing at approximately the same rate (33–35%). This behavior can be attributed to the fact that when the strains exceed the linear viscoelastic limit (such as past the yield strain), due to the large amount of deformation, different internal mechanisms can be activated that affect the CNT network, such as micro-cracking, molecular chain or nanotube slippage, interfacial debonding, or CNT rearrangement [13,23,25,65]. Once the CNT network is disrupted, the polymer matrix begins to govern the relaxation process; consequently, the relaxation behavior becomes matrix-dominated, with all nanocomposites showing similar relaxation ratio, regardless of the CNT content (Table 4).

At the 5% significance level, statistical analysis indicates that the initial strain has a significant effect on both the initial relaxation stress and long-term relaxation stress (p-value = 0.001), whereas the influence of CNT content is significant only on the long-term relaxation stress (p-value = 0.044).

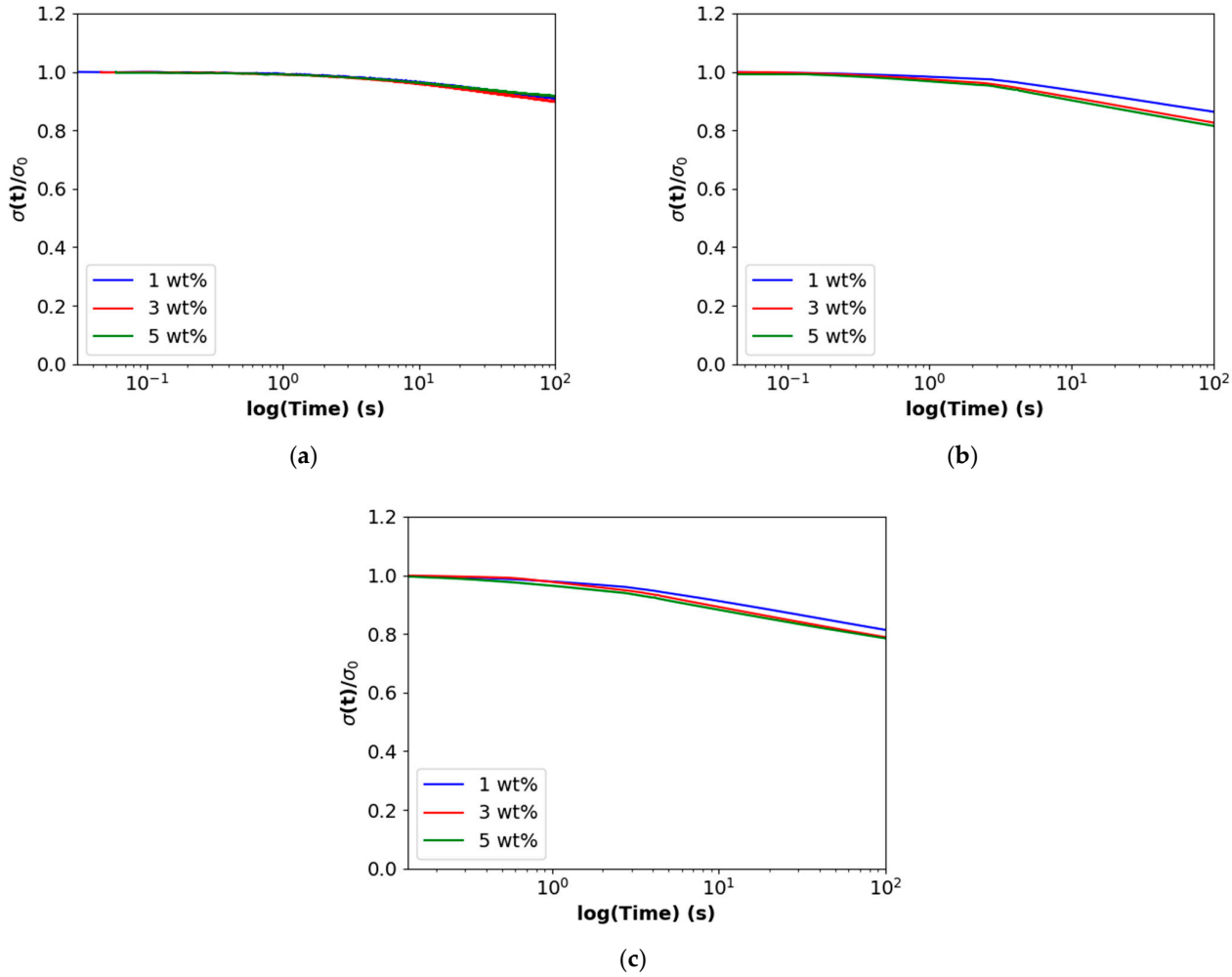


Figure 8. Normalized stress relaxation response of EVA–CNT nanocomposites during the first 100 s relaxation at (**a**) 1%, (**b**) 10%, and (**c**) 25% initial strain.

The experimental data at 1% initial strain lie within the LVR and were fitted to the generalized Maxwell model in Equation (3). The parameters τ_k (relaxation time) and E_k (relaxation modulus) were estimated by minimizing the least-squares of the residuals between the experimental data and those obtained by the developed model (Equation (10)). It should be noted that the experimental data cover 3.5 decades, and thus it was determined that four relaxation Prony terms ($N = 4$ in Equation (3)) cover the stress relaxation data. The constants determined by curve fitting the generalized Maxwell viscoelastic models along with the fitting performance (R^2 and SSq) are presented in Table 5. The tandem use of the R^2 (with a value tending to 1) and the SSq (close to 0) indicates that the Maxwell model with four Prony terms is well suited for predicting the relaxation behavior of EVA–CNT nanocomposites in the linear viscoelastic domain. Figure 9 compares the results of the Maxwell relaxation modulus to the experimental data for 1% of the initial strain.

Normalized spectra can provide information on the fraction of the initial stiffness allocated to each relaxation mode ($g_k = E_k/E_0$). Table 6 presents the normalized spectra for the EVA–CNT nanocomposites along with the equilibrium elastic fraction ($g_\infty = E_\infty/E_0$), computed based on the relaxation moduli in Table 5.

Table 5. Maxwell relaxation parameters for EVA–CNT nanocomposites: $\varepsilon_0 = 1\%$.

k	1 wt%		3 wt%		5 wt%	
	τ_k (s)	E_k (MPa)	τ_k (s)	E_k (MPa)	τ_k (s)	E_k (MPa)
1	9.56	2.28	10.71	3.80	7.01	3.00
2	58.84	3.21	71.12	4.74	38.33	4.87
3	513.97	2.30	511.12	3.57	393.49	2.14
4	3217.11	6.22	3599.98	8.34	3599.99	8.54
E_∞ (MPa)	49.20		65.58		85.22	
E_0 (MPa)	63.21		86.03		103.77	
R^2	0.999		0.999		0.999	
SSq	0.041		0.026		0.015	

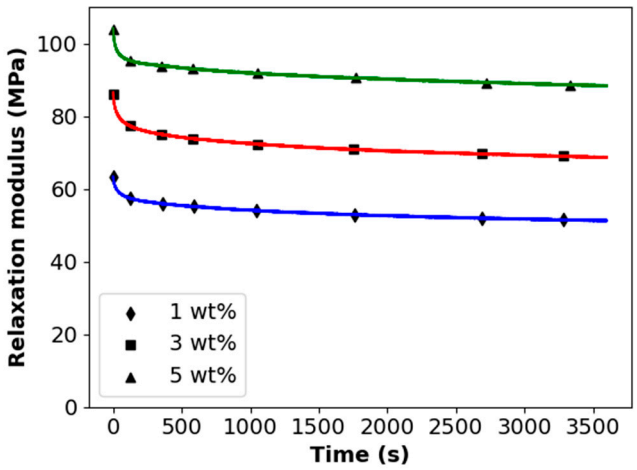


Figure 9. Predicted (symbols) and experimental (solid lines) relaxation modulus of EVA–CNT nanocomposite for 1% strain-controlled test.

Table 6. Normalized viscoelastic spectra for EVA–CNT nanocomposites: $\varepsilon_0 = 1\%$.

Parameter (%)	1 wt%	3 wt%	5 wt%	Time Domain
g_1 (instant)	3.61	4.42	2.89	Fast interfacial slippage (7–10 s)
g_2 (short)	5.08	5.51	4.69	Constrained chain segment motion (38–71 s)
g_3 (medium)	3.64	4.15	2.06	Bulk polymer chain relaxation (393–514 s)
g_4 (long)	9.84	9.69	8.23	Ultimate macromolecular alignment (3200–3600 s)
g_∞ (equilibrium)	77.84	76.23	82.12	Remaining elastic fraction

At 1% strain, the efficiency of the CNT network is considerable; at 5 wt% CNTs, the instantaneous modulus of the nanocomposite increased by about 64% (from 63 to 104 MPa) and the relaxed modulus increased by 73% (from 49 to 85 MPa) compared to the 1 wt% formulation. Moreover, the 5 wt% nanocomposite retains the highest percentage of its initial stiffness over a 1 h relaxation period, with about 82% remaining as a permanent elastic response (Table 6). The decrease in relaxation times across all three formulations may suggest the formation of an interconnected network through which a higher portion of the overall load is transferred, forcing a faster transition toward equilibrium.

The 3 wt% nanocomposite has the lowest equilibrium retention (76%) and the highest relative transient relaxation weights (g_1 to g_2), indicating that near the percolation wt%, the system is highly dynamic—yielding a higher fraction of structural relaxation.

For all three CNT contents, g_4 is the largest value; this may indicate that the bulk rearrangement of polymer chains over a long relaxation period represents the primary mechanical relaxation process.

Table 6 indicates that the nanocomposite with 5 wt% possesses very good dimensional stability (reflected by a higher g_∞ value) but lower damping capacity. On the other hand, the 3 wt% formulation exhibits the best impact absorption and energy dissipation behavior (reflected by higher g_1 to g_4 values).

While the generalized Maxwell model provides a good description of the stress relaxation behavior for EVA–CNT nanocomposites at 1% initial strain, it cannot capture their relaxation behavior at large strains (10% and 25%%). Therefore, to create an analogy with the Maxwell model, the exponential stress relaxation function (Equation (1)) with four exponential terms ($N = 4$) was used to model the experimental data at 10% and 25% strain. The fitted model parameters (τ_k and σ_k), along with the fitting performance (R^2 and SSq), are presented in Tables 7 and 8. The exponential relaxation function captures the experimental relaxation behavior of the EVA–CNT nanocomposites under large strains very well ($R^2 > 0.999$). Consequently, these model parameters can be used to predict the nonlinear stress relaxation in engineering applications when deformations exceed the LVR.

Table 7. Stress relaxation parameters for EVA–CNT nanocomposites: $\tau_k = 10\%$.

k	1 wt%		3 wt%		5 wt%	
	τ_k (s)	σ_k (MPa)	τ_k (s)	σ_k (MPa)	τ_k (s)	σ_k (MPa)
1	8.17	0.21	7.81	0.35	6.90	0.44
2	51.00	0.20	60.03	0.31	49.64	0.37
3	232.96	0.15	330.23	0.22	275.56	0.29
4	2649.06	0.41	2525.83	0.50	2500.24	0.55
σ_∞ (MPa)	2.45		2.80		3.43	
σ_0 (MPa)	3.42		4.17		5.07	
R^2	1.000		0.999		1.000	
SSq	0.002		0.004		0.002	

Table 8. Stress relaxation parameters for EVA–CNT nanocomposites: $\varepsilon_0 = 25\%$.

k	1 wt%		3 wt%		5 wt%	
	τ_k (s)	σ_k (MPa)	τ_k (s)	σ_k (MPa)	τ_k (s)	σ_k (MPa)
1	7.20	0.34	6.73	0.59	5.97	0.68
2	47.98	0.33	51.39	0.47	44.16	0.54
3	248.52	0.30	293.46	0.38	247.73	0.41
4	2402.20	0.48	2704.13	0.59	2152.91	0.59
σ_∞ (MPa)	2.75		3.46		4.37	
σ_0 (MPa)	4.20		5.49		6.60	
R^2	1.000		1.000		1.000	
SSq	0.003		0.004		0.004	

5. Summary and Conclusions

In this study, the stress relaxation behavior of EVA–CNT nanocomposites with 1, 3, and 5 wt% CNTs was analyzed under small and large strains using two different experimental modes, such as load- and strain- controlled uniaxial tensile tests. The experimental stress relaxation data were fitted to the generalized Maxwell linear viscoelastic model, and the Prony relaxation parameters were calculated using the nonlinear least-squares method. The main findings from the study are as follows:

- The stress relaxation response of the three EVA–CNT nanocomposites (1, 3 and 5 wt%) remains within the LVR up to a 6% strain and exhibits a clear transition to non-linear behavior at higher strains (near or above the yield point).
- The generalized Maxwell model accurately captured the relaxation behavior of EVA–CNT nanocomposites within the LVR, providing a robust fit for experimental relaxation data with relative errors not exceeding 5%.
- Within the LVR, the EVA–CNT nanocomposites retain at least 70–80% of their instantaneous modulus. More importantly, increasing the CNT content from 1 to 5 wt% nearly doubled the equilibrium modulus, yielding a 1.70- to 1.85-fold increase depending on the initial strain and relaxation period.
- Under high strains (10% and 25%), the relaxation behavior of EVA–CNT nanocomposites became matrix-dominant, with all three formulations exhibiting a similar stress relaxation ratio of 30–35%.
- From a practical point of view, the nanocomposite with 5 wt% exhibits very good dimensional stability but lower damping capacity. Conversely, if the application requires impact absorption or energy dissipation, the nanocomposite with 3 wt% is the best candidate.

The present modeling framework assumes linear viscoelastic behavior, and the material parameters in terms of Maxwell relaxation modulus are reliable within the spectrum of strain or load levels used during the original experimental curve-fitting process. However, during a given application, the nanocomposites can be subjected to different types of loads or strains that may exceed the purely viscoelastic domain, and the generalized Maxwell model cannot be applied for capturing the relaxation response. Therefore, future work will investigate the applicability of other relaxation models, including nonlinear Maxwell and non-Maxwellian viscoelastic models, to capture stress relaxation behavior under large strains. In addition, as the properties of these nanocomposites extend across different scales, future work will address time-dependent behavior at micro- and nanoscales.

Author Contributions: Conceptualization, F.S., S.C. and C.F.; methodology, F.S., I.-L.S., S.C. and C.F.; software, F.S. and S.C.; validation, F.S., S.C.; formal analysis, F.S., I.-L.S. and C.F.; investigation, F.S., I.-L.S. and C.F.; resources, F.S., C.F.; data curation, F.S. and S.C.; writing—original draft preparation, F.S.; writing—review and editing, F.S., S.C., I.-L.S. and C.F.; visualization, F.S. and S.C.; supervision, F.S. and C.F.; project administration, F.S., I.-L.S. and C.F.; funding acquisition, F.S., I.-L.S. and C.F. All authors have read and agreed to the published version of the manuscript.

Funding: This work was partially supported by an internal research grant from Dunarea de Jos University of Galati, contract number 7968/31.03.2025.

Data Availability Statement: The original contributions presented in this study are included in the article. Further inquiries can be directed to the corresponding authors.

Conflicts of Interest: The authors declare no conflicts of interest.

References

1. Dassan, E.G.B.; Ab Rahman, A.A.; Abidin, M.S.Z.; Akil, H.M. Carbon nanotube–reinforced polymer composite for electromagnetic interference application: A review. *Nanotechnol. Rev.* **2020**, *9*, 768–788. [CrossRef]
2. Soni, S.K.; Thomas, B.; Kar, V.R. A comprehensive review on CNTs and CNT-reinforced composites: Syntheses, characteristics and applications. *Mater. Today Commun.* **2020**, *25*, 101546. [CrossRef]
3. Murjani, B.O.; Kadu, P.S.; Bansod, M.; Vaidya, S.S.; Yadav, M.D. Carbon nanotubes in biomedical applications: Current status, promises, and challenges. *Carbon Lett.* **2022**, *32*, 1207–1226. [CrossRef] [PubMed]
4. Ali, Z.; Yaqoob, S.; Yu, J.; D'Amore, A. Critical review on the characterization, preparation, and enhanced mechanical, thermal, and electrical properties of carbon nanotubes and their hybrid filler polymer composites for various applications. *Compos. C Open Access* **2024**, *13*, 100434. [CrossRef]

5. Fenta, E.W.; Mebratie, B.A. Advancements in carbon nanotube-polymer composites: Enhancing properties and applications through advanced manufacturing techniques. *Heliyon* **2024**, *10*, e36490. [CrossRef] [PubMed]
6. Tan, J.; Zhang, Y. Thermal conductive polymer composites: Recent progress and applications. *Molecules* **2024**, *29*, 3572. [CrossRef] [PubMed]
7. Yim, Y.J.; Yoon, Y.H.; Kim, S.H.; Lee, J.H.; Chung, D.C.; Kim, B.J. Carbon nanotube/polymer composites for functional applications. *Polymers* **2025**, *17*, 119. [CrossRef] [PubMed]
8. Sabet, M. Innovations in carbon nanotube polymer composites: Electrical, thermal, and mechanical advancements for aerospace and automotive applications. *Synth. Met.* **2025**, *310*, 117794. [CrossRef]
9. Shchegolkov, A.V.; Shchegolkov, A.V.; Kaminskii, V.V.; Iturralde, P.; Chumak, M.A. Advances in electrically and thermally conductive functional nanocomposites based on carbon nanotubes. *Polymers* **2025**, *17*, 71. [CrossRef] [PubMed]
10. Omana, L.; Chandran, A.; John, R.E.; Wilson, R.; George, K.C.; Unnikrishnan, N.V.; Varghese, S.S.; George, G.; Simon, S.M.; Paul, I. Recent advances in polymer nanocomposites for electromagnetic interference shielding: A review. *ACS Omega* **2022**, *7*, 25921–25947. [CrossRef] [PubMed]
11. Xia, H.; Song, M.; Zhang, Z.; Richardson, M. Microphase separation, stress relaxation, and creep behavior of polyurethane nanocomposites. *J. Appl. Polym. Sci.* **2007**, *103*, 2992–3002. [CrossRef]
12. Wang, L.; Han, Y. Compressive relaxation of the stress and resistance for carbon nanotube filled silicone rubber composite. *Compos.-A Appl. Sci. Manuf.* **2013**, *47*, 63–71. [CrossRef]
13. Maria, H.J.; Lyczko, N.; Nzihou, A.; Joseph, K.; Mathew, C.; Thomas, S. Stress relaxation behavior of organically modified montmorillonite filled natural rubber/nitrile rubber nanocomposites. *Appl. Clay Sci.* **2014**, *87*, 120–128. [CrossRef]
14. Georgousis, G.; Pandis, C.; Kalamiotis, A.; Georgiopoulos, P.; Kyritsis, A.; Kontou, E.; Pissis, P.; Micusik, M.; Czanikova, K.; Kulicek, J.; et al. Strain sensing in polymer/carbon nanotube composites by electrical resistance measurement. *Compos. B Eng.* **2015**, *68*, 162–169. [CrossRef]
15. Michardiere, A.S.; Mateo-Mateo, C.; Derre, A.; Correa-Duarte, M.A.; Mano, N.; Poulin, P. Carbon nanotube microfiber actuators with reduced stress relaxation. *J. Phys. Chem. C* **2016**, *120*, 6851–6858. [CrossRef]
16. Oseli, A.; Vesel, A.; Zagar, E.; Perse, L.S. Mechanisms of single-walled carbon nanotube network formation and its configuration in polymer-based nanocomposites. *Macromolecules* **2021**, *54*, 3334–3346. [CrossRef]
17. Shim, W.; Jeon, S.Y.; Yu, W.R. Modeling of the piezoresistive behavior of carbon nanotube/polymer composites during stress relaxation. *Polym. Compos.* **2022**, *43*, 2672–2682. [CrossRef]
18. Raj, G.B.; Saludheen, A.; Arumugham-Achari, A.K.; George, N.; Chacko, T. Simulations for mechanical properties of polymer composites: Investigations into suitability of numerical models for TPU-CNT with Mooney–Rivlin (N = 1) and friction. *Mech. Time-Depend. Mater.* **2023**, *27*, 705–726. [CrossRef]
19. Huang, J.; Zhou, H.; Zhang, L.; Zhang, L.; Shi, W.; Yang, Y.; Zhou, J.; Zhao, T.; Liu, M. Full-scale polymer relaxation induced by single-chain confinement enhances mechanical stability of nanocomposites. *Nat. Commun.* **2024**, *15*, 6747. [CrossRef] [PubMed]
20. Yazdanparast, R.; Rafiee, R. A 3D viscoelastic–viscoplastic behavior of carbon nanotube-reinforced polymers: Constitutive model and experimental characterization. *Polym. Compos.* **2024**, *45*, 6425–6438. [CrossRef]
21. Xu, Q.; Qu, H.; Wu, Z.; Zhao, Z.; Ge, S.; Luo, J.; Zuo, B. Relaxation-enhanced polymer nanocomposites induced by bound polymer loops on the particle surfaces. *Nat. Commun.* **2025**, *16*, 9870. [CrossRef] [PubMed]
22. Costa, P.; Nunes-Pereira, J.; Silva, A.P.; Lanceros-Mendez, S. On the mechanical and electrical relaxation in piezoresistive polymer composites. *Compos.-A Appl. Sci. Manuf.* **2026**, *205*, 109695. [CrossRef]
23. Yao, Z.; Wu, D.; Chen, C.; Zhang, M. Creep behavior of polyurethane nanocomposites with carbon nanotubes. *Compos.-A Appl. Sci. Manuf.* **2013**, *50*, 65–72. [CrossRef]
24. Pan, Y.; Weng, G.J.; Meguid, S.A.; Bao, W.S.; Zhu, Z.H.; Hamouda, A.M.S. Interface effects on the viscoelastic characteristics of carbon nanotube polymer matrix composites. *Mech. Mater.* **2013**, *58*, 1–11. [CrossRef]
25. Ansari, R.; Hassanzadeh-Aghdam, M.K. Micromechanical investigation of creep-recovery behavior of carbon nanotube-reinforced polymer nanocomposites. *Int. J. Mech. Sci.* **2016**, *115*, 45–55. [CrossRef]
26. Hassanzadeh-Aghdam, M.K.; Mahmoodi, M.J.; Ansari, R. Creep performance of CNT polymer nanocomposites-An emphasis on viscoelastic interphase and CNT agglomeration. *Compos. B Eng.* **2019**, *168*, 274–281. [CrossRef]
27. Obaid, N.; Kortschot, M.T.; Sain, M. Understanding the stress relaxation behavior of polymers reinforced with short elastic fibers. *Materials* **2017**, *10*, 472. [CrossRef] [PubMed]
28. Obaid, N.; Kortschot, M.T.; Sain, M. Predicting the stress relaxation behavior of glass-fiber reinforced polypropylene composites. *Compos. Sci. Technol.* **2018**, *161*, 85–91. [CrossRef]
29. Huang, J.; Zhou, J.; Liu, M. Interphase in polymer nanocomposites. *JACS Au* **2022**, *2*, 280–291. [CrossRef] [PubMed]
30. Stan, F.; Stanciu, N.V.; Constantinescu, A.M.; Fetecau, C. 3D printing of flexible and stretchable parts using multiwall carbon nanotube/polyester-based thermoplastic polyurethane. *J. Manuf. Sci. Eng. Trans. ASME* **2021**, *143*, 051002. [CrossRef]

31. Wang, X.; Lim, E.G.; Hoettges, K.; Song, P. A review of carbon nanotubes, graphene and nanodiamond based strain sensor in harsh environments. *C* **2023**, *9*, 108. [CrossRef]
32. Jia, B.; Liu, Z.; Xiang, D.; Liu, L.; Sun, H.; Wu, Y.; Mu, M.; Wang, B.; Zhao, C.; Li, H. Flexible strain sensors based on carbon nanotubes/polydimethylsiloxane composites with a segregated structure prepared by sustainable emulsion method. *Polym. Eng. Sci.* **2025**, *65*, 1093–1105. [CrossRef]
33. Alqaderi, A.I.; Ramakrishnan, N. Carbon-based flexible strain sensors: Recent advances and performance insights in human motion detection. *Chem. Eng. J.* **2025**, *513*, 162609. [CrossRef]
34. Hakim, M.L.; Alfarros, Z.; Herianto, H.; Muflikhun, M.A. High sensitivity flexible strain sensor for motion monitoring based on MWCNT@ MXene and silicone rubber. *Sci. Rep.* **2025**, *15*, 3741. [CrossRef] [PubMed]
35. Shchegolkov, A.V.; Shchegolkov, A.V.; Kaminskii, V.V. Carbon nanotubes and graphene in polymer composites for strain sensors: Synthesis, functionalization, and application. *J. Compos. Sci.* **2026**, *10*, 43. [CrossRef]
36. Sabet, M.; Soleimani, H.; Hosseini, S. Properties and characterization of ethylene-vinyl acetate filled with carbon nanotube. *Polym. Bull.* **2016**, *73*, 419–434. [CrossRef]
37. Rosculet, R.T.; Stan, F.; Fetecau, C. On the strain sensing of EVA/MWCNT composite. *Mater. Plast.* **2018**, *55*, 274–278. [CrossRef]
38. Stanciu, N.V.; Stan, F.; Sandu, I.L.; Susac, F.; Fetecau, C.; Rosculet, R.T. Mechanical, electrical and rheological behavior of ethylene-vinyl acetate/multi-walled carbon nanotube composites. *Polymers* **2019**, *11*, 1300. [CrossRef] [PubMed]
39. Sandu, I.L.; Stan, F.; Fetecau, C. Mechanical recycling of ethylene-vinyl acetate/carbon nanotube nanocomposites: Processing, thermal, rheological, mechanical and electrical behavior. *Polymers* **2023**, *15*, 583. [CrossRef] [PubMed]
40. Li, Z.; Qi, X.; Xu, L.; Lu, H.; Wang, W.; Jin, X.; Islam Md, Z.; Zhu, Y.; Fu, Y.; Ni, Q.; et al. Self-repairing, large linear working range shape memory carbon nanotubes/ethylene vinyl acetate fiber strain sensor for human movement monitoring. *ACS Appl. Mater. Interfaces* **2020**, *12*, 42179–42192. [CrossRef] [PubMed]
41. Xiang, D.; Li, J.; Li, Z.; Zhang, X.; Zhao, C.; Li, H.; Lai, J.; Wang, B.; Wang, P.; Li, D.; et al. Bilayer-structured carbon nanotube/ethylene–vinyl acetate flexible strain sensors with enhanced sensing performance prepared by biaxial stretching. *Sens. Actuators A Phys.* **2024**, *366*, 114992. [CrossRef]
42. Xie, M.; Li, S.; Qi, X.; Chi, Z.; Shen, L.; Islam, Z.; Dong, Y. Thermal and infrared light self-repairing, high sensitivity, and large strain sensing range shape memory MXene/CNTs/EVA composites fiber strain sensor for human motion monitoring. *Sens. Actuators A Phys.* **2022**, *347*, 113939. [CrossRef]
43. Wang, S.; Wang, W.; Chi, Z.; Long, Z.; Xu, H.; Dong, Y. Development of electric-and near-infrared light-driven CNTs/EVA shape memory composite actuators with strain sensing and encrypted information transmitting functionalities. *Sens. Actuators A Phys.* **2023**, *360*, 114547. [CrossRef]
44. Shi, J.; Chen, N.; Tian, J.; Gu, J.; Sun, H.; Zeng, H. Investigation of thermomechanical one-way and two-way shape memory behaviors of crosslinked poly (ethylene-co-vinyl acetate)/multi-walled carbon nanotube composites. *Smart Mater. Struct.* **2025**, *34*, 065022. [CrossRef]
45. Tang, J.; Lin, C.; Duan, C.; Nie, L.; Han, L. Impact of Aligned Carbon Nanotubes on the Mechanical Properties and Sensing Performance of EVA/CNTs Composites. *Mater. Plast.* **2024**, *61*, 90–100. [CrossRef]
46. Lian, Y.; Li, Z.; Bowen, C.; Roscow, J.; Wemyss, A.M.; Wan, C. Microcellular Poly (Ethylene-Co-Vinyl Acetate)/Lignin Nanocomposites for Soft Ferroelectrets. *Adv. Eng. Mater.* **2025**, *27*, 2501268. [CrossRef]
47. Chang, B.P.; Kashcheev, A.; Veksha, A.; Lisak, G.; Goei, R.; Leong, K.F.; Tok, A.I.Y.; Lipik, V. Nanocomposite foams with balanced mechanical properties and energy return from EVA and CNT for the midsole of sports footwear application. *Polymers* **2023**, *15*, 948. [CrossRef] [PubMed]
48. Zubkiewicz, A.; Szymczyk, A.; Franciszczak, P.; Kochmanska, A.; Janowska, I.; Paszkiewicz, S. Comparing multi-walled carbon nanotubes and halloysite nanotubes as reinforcements in EVA nanocomposites. *Materials* **2020**, *13*, 3809. [CrossRef] [PubMed]
49. Al-Fawzan, F.F.; Abd El-Gawad, A.F.; Fayek, S.A.; Saleh, M.G.; Al-Khazaal, A.Z.; Alahmadi, N.; Sharshir, A.I. Tuning electrical properties of EVA polymer film by dual-doping CNT and SnO_2 for cable applications. *Solid State Sci.* **2026**, *175*, 108255. [CrossRef]
50. Alcudia® PA-420 Datasheet. Available online: https://www.repsol.com/ (accessed on 23 July 2019).
51. NC7000TM Datasheet. Available online: https://www.birlacarbon.com/wp-content/uploads/hse/nanocyl/dm-ti-02-tds-nc7000-v08.pdf (accessed on 1 September 2026).
52. *ISO 527-1:2019*; Plastics—Determination of Tensile Properties. ISO—International Organization for Standardization: Geneva, Switzerland, 2019.
53. Shaw, M.T.; MacKnight, W.J. *Introduction to Polymer Viscoelasticity*, 3rd ed.; Wiley-Interscience: Hoboken, NJ, USA, 2005.
54. Jalocha, D.; Constantinescu, A.; Neviere, R. Revisiting the identification of generalized Maxwell models from experimental results. *Int. J. Solids Struct.* **2015**, *67*, 169–181. [CrossRef]
55. Gebrehiwot, S.Z.; Espinosa-Leal, L. Characterising the linear viscoelastic behaviour of an injection moulding grade polypropylene polymer. *Mech. Time-Depend. Mater.* **2022**, *26*, 791–814. [CrossRef]
56. Betten, J. Viscoelastic Materials. In *Creep Mechanics*, 3rd ed.; Springer: Berlin/Heidelberg, Germany, 2008; pp. 195–244.

57. Saprunov, I.; Gergesova, M.; Emri, I. Prediction of viscoelastic material functions from constant stress-or strain-rate experiments. *Mech. Time-Depend. Mater.* **2014**, *18*, 349–372. [CrossRef]
58. Ciambella, J.; Paolone, A.; Vidoli, S. A comparison of nonlinear integral-based viscoelastic models through compression tests on filled rubber. *Mech. Mater.* **2010**, *42*, 932–944. [CrossRef]
59. Tschoegl, N.W. *The Phenomenological Theory of Linear Viscoelastic Behavior: An Introduction*; Springer: Berlin, Germany, 1989.
60. The MathWorks Inc. *MATLAB*, version R2025a; The MathWorks Inc.: Natick, MA, USA, 2025.
61. Knauss, W.G.; Zhao, J. Improved relaxation time coverage in ramp-strain histories. *Mech. Time-Depend. Mater.* **2007**, *11*, 199–216. [CrossRef]
62. Baumgaertel, M.; Winter, H.H. Determination of discrete relaxation and retardation time spectra from dynamic mechanical data. *Rheol. Acta.* **1989**, *28*, 511–519. [CrossRef]
63. Mičušík, M.; Omastová, M.; Krupa, I.; Prokeš, J.; Pissis, P.; Logakis, E.; Pandis, C.; Pötschke, P.; Pionteck, J.; Pionteck, J. A comparative study on the electrical and mechanical behaviour of multi-walled carbon nanotube composites prepared by diluting a masterbatch with various types of polypropylenes. *J. Appl. Polym. Sci.* **2009**, *113*, 2536–2551. [CrossRef]
64. Ghosh, R.; Misra, A. Tailored viscoelasticity of a polymer cellular structure through nanoscale entanglement of carbon nanotubes. *Nanoscale Adv.* **2020**, *2*, 5375–5383. [CrossRef] [PubMed]
65. Yang, J.; Zhang, Z.; Friedrich, K.; Schlarb, A.K. Creep resistant polymer nanocomposites reinforced with multiwalled carbon nanotubes. *Macromol. Rapid Commun.* **2007**, *28*, 955–961. [CrossRef]
66. Qian, D.; Dickey, E.C. In-situ transmission electron microscopy studies of polymer–carbon nanotube composite deformation. *J. Microsc.* **2001**, *204*, 39–45. [CrossRef] [PubMed]
67. Kuronuma, Y.; Shindo, Y.; Takeda, T.; Narita, F. Crack growth characteristics of carbon nanotube-based polymer composites subjected to cyclic loading. *Eng. Fract. Mech.* **2011**, *78*, 3102–3110. [CrossRef]
68. Flory, A.; McKenna, G.B. Finite step rate corrections in stress relaxation experiments: A comparison of two methods. *Mech. Time-Depend. Mater.* **2004**, *8*, 17–37. [CrossRef]
69. Du, M.; Wang, Y.; Wang, Z. Effect of the initial ramps of creep and relaxation tests on models with fractional derivatives. *Meccanica* **2017**, *52*, 3541–3547. [CrossRef]

Disclaimer/Publisher's Note: The statements, opinions and data contained in all publications are solely those of the individual author(s) and contributor(s) and not of MDPI and/or the editor(s). MDPI and/or the editor(s) disclaim responsibility for any injury to people or property resulting from any ideas, methods, instructions or products referred to in the content.